Bubble Growth in the Microcellular Foaming of CO_2/Polypropylene Solutions

Ping Zhang,[1] Xiao-Jun Wang,[1] Yong Yang,[1] Nan-Qiao Zhou[2]

[1]*College of Electromechanical Engineering, GuangDong Polytechnic Normal University, GuangZhou 510665, China*
[2]*National Engineering Research Center of Novel Equipment for Polymer Processing, Key Laboratory of Polymer Processing Engineering, Ministry of Education, South China University of Technology, Guanzhou 510640, China*

Received 18 August 2008; accepted 8 April 2009
DOI 10.1002/app.30648
Published online 10 June 2010 in Wiley InterScience (www.interscience.wiley.com).

ABSTRACT: This article is concerned with bubble growth dynamics in the CO_2/polypropylene microcellular foaming process. The effect of the melt strength on the bubble growth was thoroughly investigated in theory for the first time. The theoretical results indicate that enhanced melt strength effectively restrains the bubble growth and stabilizes the bubble oscillation. Higher melt strength leads to lower bubble growth rate, shorter growth time, and smaller ultimate bubble size. Compared to the melt strength, the viscoelasticity and the gas pressure have less effect on the microcellular foaming process. The bubble growth varies a little as the viscoelasticity is varied. The bubble oscillation and growth rate are enhanced with increasing gas pressure, which leads to the augmentation of the bubble size. © 2010 Wiley Periodicals, Inc. J Appl Polym Sci 118: 1949–1955, 2010

Key words: growth; poly(propylene) (PP); theory

INTRODUCTION

The melt strength of a polymer is a measurement of its resistance to extensional deformation.[1] It is an important processing parameters in melt processing where stretching or drawing occurs, such as in melt spinning, blow molding, extrusion coating, and fiber extrusion. The melt strength is recognized as the key parameter in polymer foaming because of its great effect on bubble growth (or collapse) and ultimate bubble size. Lee et al.[2] reported that the polymer melt near the gas bubbles was stretched biaxially when the gas bubbles grew. The melt tension of the polymer around the bubble played an important role in restraining the bubble growth and preventing the breaking of the gas bubbles. The bubble size and foaming degree decreased with increasing melt tension of the polymer regardless of the structure, molecular weight of the polymer resin, and melt temperature. It is known that common polypropylene (PP) has a low melt strength and poor foamability because of its crystallizability and linear molecular structure. It is usually chemically or physically modified to enhance the melt strength and improve the foamability.

Correspondence to: P. Zhang (cathyzp2002@163.com).
Contract grant sponsor: Foundation of Cultivating Excellent and Innovational Young People of Guangdong Province; contract grant number: LYM08073.

Microcellular foaming is a complex process, for many variables simultaneously influence the rheology and microstructure of the foam product. Bubble growth is one of the most important stages of the foaming process because of its close relationship with the ultimate bubble size and the microstructure. It has been broadly investigated since 1917. Bubble growth models can be classified into two groups: single-bubble growth models[3–5] and cell models.[6–8]

Zana and Leal[9] investigated the effect of the shear viscosity and surface tension on bubble collapse using a single-bubble growth model. They reported that the internal gas pressure and bubble collapse rate decreased as the viscosity increased or the surface tension decreased. Arefmanesh and coworkers[6,7] studied the influence of the dimensionless parameters of the structure foam processing on the bubble growth in viscoelastic and Newtonian fluids using the cell model. They reported that the bubble growth rate in the viscoelastic medium was higher than that in the Newtonian medium during the early stage of the bubble growth. However, the fluid elasticity had little effect on the bubble growth in the latter stage. The ultimate foam had the same steady-state configuration in the viscoelastic and Newtonian fluids. The bubble growth and cellular structure in viscoelastic media were predicted in refs. 10 and 11. The results show that the bubble growth rate increased with increasing gas solubility, pressure gradient across the bubble surface, and elastic-to-viscous ratio.

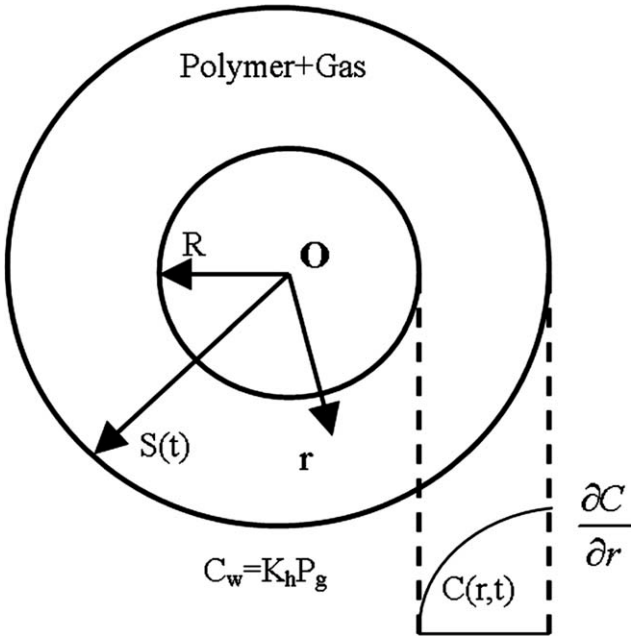

Figure 1 Cell model of the bubble growth. C_w is the gas concentration at the bubble interface.

Lowering the surface tension increased the nucleation rate, which led to a higher bubble density, smaller bubble size, and narrower bubble size distribution.

Although the melt strength plays a very important role in the foaming process, its effect on bubble growth has not been theoretically investigated to any great degree. Deeply and comprehensive experimental studies have not yet been carried out. In this study, the effects of parameters, including the melt strength, on the bubble growth were theoretically investigated and simulated with a cell model, and the results are analyzed and compared in detail and comprehensively in this article.

BUBBLE GROWTH DYNAMICS

Mathematical model

A numerical simulation model was constructed to illustrate bubble growth in foam processing after bubble nucleation. Consider a bubble concentrically surrounded by a shell of polymer melt with a constant mass. The gas dissolved in the melt shell uniformly distributes in a saturation state at the initial time and only diffuses between the melt shell and the bubble during bubble growth. Figure 1 shows the configuration of the bubble and the melt shell surrounding the bubble. The spherical coordinate was selected with the center of the bubble as the origin. In Figure 1, R is the bubble radius, S is the outer radius of the melt shell, r is the radial coordinate in the spherical region, and c is the concentration of the dissolved gas in the melt.

Before analyzing the bubble growth, we made the following assumptions:

1. The bubble and the melt shell had the same and fixed sphere center throughout the growth period.
2. The gravity and inertia effects were ignored because of the highly viscous entangled polymer melt.
3. The polymer melt was incompressible. The volume of dissolved gas in the melt was negligible.
4. Because the timescale of the bubble expansion was much shorter than the cooling time, the growth process was considered to be isothermal.
5. The dissolved gas in the polymer melt was in the uniformly supersaturated state before bubble growth.
6. The dissolved gas did not go in and out at the outer boundary of the analyzed region.

Melt strength formation

When the polymer melt is stretched or drawn, a melt strength forms in the polymer melt to resist the tensile force. As the bubble grows, the melt shell surrounding the bubble is stretched biaxially under the high pressure inside the bubble, and melt strength forms in the melt shell.[2] The melt strength, surface tension, and ambient pressure around the melt shell (P_f) restrain the bubble expansion. That is, the melt strength is a force to resist the bubble growth.[12] The surface tension is the force per unit length[12] that is tangent to the interface. Referring to the definition of the surface tension, we define melt tension as the melt strength per unit area (ξ) that is tangent to the melt shell. The melt shell around the bubble is considered to consist of coaxial infinitely thin melt spheres. The melt tension of each sphere is equal because the growth process is isothermal. According to refs. 12 and 13, in a melt sphere with radius r and thickness (dr), the radial pressure drop (dp) caused by the melt tension is

$$dp = \frac{2\xi dr}{r} \tag{1}$$

The integration of eq. (1) over r from the bubble surface to the outer boundary of the melt shell results in the whole radial pressure drop around the melt shell:

$$\int_R^S \frac{2\xi dr}{r} = 2\xi \ln \frac{S}{R} \tag{2}$$

The gas pressure inside the bubble (P_g) equals the whole pressure of the melt shell, which takes the following form:

$$P_g = \frac{2\sigma}{R} + 2\xi \ln\frac{S}{R} + P_f \tag{3}$$

where σ is the surface tension.

In view of the previous assumptions, the equations of the force balance at the bubble surface and outer boundary of the melt shell take the following forms:

$$P_g + \tau_{rr}(R) = \frac{2\sigma}{R} + P(R) \tag{4}$$

$$P(S) = P_f + \tau_{rr}(S) \tag{5}$$

where τ_{rr} is the normal component of the stress tensor and P is the melt pressure.

Basic governing equations of the bubble growth

Continuity equation

The continuity equation in spherical coordinates is given by

$$\nabla \cdot \vec{V} = \frac{\partial r^2 V_r}{r^2 \partial r} = 0 \tag{6}$$

where V is the velocity vector of the fluid and V_r is the radial velocity of the liquid. At the interface of the bubble and the melt shell, eq. (6) may be simplified to

$$V_r = \frac{R^2 \dot{R}}{r^2} \tag{7}$$

where $\dot{R}$ is the radial bubble velocity.

Momentum equation

The momentum equation in the radial direction for the spherical coordinates is expressed as

$$-\frac{\partial P}{\partial r} + \frac{1}{r^2}\frac{\partial (r^2 \tau_{rr})}{\partial r} - \frac{2\tau_{\theta\theta}}{r} = 0 \tag{8}$$

Equation (8) can be switched to

$$-\frac{\partial P}{\partial r} + \frac{\partial \tau_{rr}}{\partial r} + \frac{2}{r}(\tau_{rr} - \tau_{\theta\theta}) = 0 \tag{9}$$

On integrating eq. (9) over r from the bubble surface to the outer boundary of the melt shell, one obtains

$$-P(S) + P(R) + \tau_{rr}(S) - \tau_{rr}(R) + 2\int_R^S \frac{\tau_{rr} - \tau_{\theta\theta}}{r} dr = 0 \tag{10}$$

Substituting eqs. (2), (4), and (5) into eq. (10), one can obtain

$$2P_g - 2P_f - \frac{4\sigma}{R} - 2\xi 1n\frac{S}{R} + 2\int_R^S \frac{\tau_{rr} - \tau_{\theta\theta}}{r} dr = 0 \tag{11}$$

Differential mass balance

To calculate the gas concentration within the melt shell and P_g, a gas diffusion equation in the spherical coordinate is introduced,[8,14] namely

$$\frac{\partial C}{\partial t} + V_r \frac{\partial C}{\partial r} = \frac{D}{r^2}\frac{\partial}{\partial r}\left(r^2 \frac{\partial C}{\partial r}\right) \quad R(t) \le r \le S \tag{12}$$

where C is CO_2 concentration dissolved in the polymer melt, and t is the gas diffusion time in the melt. The initial and boundary conditions for eq. (12) are

$$C(r, 0) = C_0 \qquad (R \le r \le S) \tag{13}$$

$$\left.\frac{\partial C}{\partial r}\right|_{r=s} = 0 \tag{14}$$

$$C_R(R, t) = K_h P_g \tag{15}$$

where $C(r,t)$ is the CO_2 concentration dissolved in the polymer melt, D is the diffusion coefficient, C_R is the gas concentration at the bubble interface, and K_h is the Henry's law constant.

The conservation of mass inside the bubble is[15]

$$\frac{d}{dt}\left(\frac{4\pi}{3}\rho_g R^3\right) = 4\pi\rho D R^2 \left.\frac{\partial C}{\partial r}\right|_{r=R} \tag{16}$$

where ρ_g is the gas density and ρ is the melt density.

To simplify the calculation,[14,16] the gas in the bubble is assumed to follow the ideal gas law:

$$\rho_g = \frac{P_g M}{R_g T} \tag{17}$$

where R_g is the molar gas constant, M is the molecular weight of the gas, and T is the temperature.

The substitution of eq. (17) into eq. (16) results in

$$\frac{d}{dt}\left(\frac{P_g M R^3}{R_g T}\right) = 3\rho D R^2 \left.\frac{\partial C}{\partial r}\right|_{r=R} \tag{18}$$

Constitutive equation

According to the characteristics of the foaming liquid, we first refer to the Dewitt viscoelastic model,[5,17,18] which describes the important viscoelastic properties of the polymer, such as stress, stress relaxation, and viscosity. It may be represented as

$$\vec{\tau} + \lambda \frac{D\vec{\tau}}{Dt} = \eta \vec{d} \tag{19}$$

where τ is the stress tensor, η is the viscosity, λ is the relaxation time, and $\vec{d}$ is the strain-rate tensor and can be written as

$$\vec{d} = \frac{1}{2}\begin{bmatrix} 2\frac{\partial V_r}{\partial r} & r\frac{\partial}{\partial r}\left(\frac{V_\theta}{r}\right) + \frac{1}{r}\frac{V_r}{\partial\theta} & \frac{1}{r\sin\theta}\frac{\partial V_r}{\partial\phi} + r\frac{\partial}{\partial r}\left(\frac{V_\phi}{r}\right) \\ r\frac{\partial}{\partial r}\left(\frac{V_\theta}{r}\right) & 2\left(\frac{V_r}{r} + \frac{1}{r}\frac{\partial V_\theta}{\partial\theta}\right) & \frac{\sin\theta}{r}\frac{\partial}{\partial\theta}\left(\frac{V_\phi}{\sin\theta} + \frac{1}{r\sin\theta}\frac{\partial V_\theta}{\partial\phi}\right) \\ 0 & 0 & 2\left(\frac{1}{r\sin\theta}\frac{\partial V_\phi}{\partial\phi} + \frac{V_r}{r} + \frac{V_\theta \mathrm{ctg}\theta}{r}\right) \end{bmatrix} \tag{20}$$

where θ is the angle in the horizontal direction in polar coordinates, ϕ is the angle in the vertical direction in polar coordinates, V_θ is the liquid velocity in the direction of angle θ in polar coordinates, and $V\phi$ is the liquid velocity in the direction of angle ϕ in polar coordinates.

The substitution of $V_\theta = V_\phi = 0$ and $V_r = (R^2\dot{R}/r)^2$ into eq. (20) results in

$$\vec{d} = \begin{bmatrix} \frac{\partial V_r}{\partial r} & 0 & 0 \\ 0 & \frac{V_r}{r} & 0 \\ 0 & 0 & \frac{V_r}{r} \end{bmatrix} = \begin{bmatrix} -\frac{2R^2\dot{R}}{r^3} & 0 & 0 \\ 0 & \frac{R^2\dot{R}}{r^3} & 0 \\ 0 & 0 & \frac{R^2\dot{R}}{r^3} \end{bmatrix} \tag{21}$$

The stress tensor ($\vec{\tau}$) can be expressed as

$$\vec{\tau} = \begin{bmatrix} \tau_{rr} & 0 & 0 \\ 0 & \tau_{\theta\theta} & 0 \\ 0 & 0 & \tau_{\phi\phi} \end{bmatrix} \tag{22}$$

where $\tau_{\theta\theta}$ is the stress tensor in the direction of angle ϕ in polar coordinates. The integration of eqs. (21), (22), and (19) results in

$$\tau_{rr} + \lambda\left[\frac{\partial\tau_{rr}(r,t)}{\partial t} + \frac{R^2\dot{R}}{r^2}\frac{\partial\tau_{rr}(r,t)}{\partial r}\right] = -2\eta\frac{R^2\dot{R}}{r^3} \tag{23}$$

$$\tau_{\theta\theta} + \lambda\left[\frac{\partial\tau_{\theta\theta}(r,t)}{\partial t} + \frac{R^2\dot{R}}{r^2}\frac{\partial\tau_{\theta\theta}(r,t)}{\partial r}\right] = \eta\frac{R^2\dot{R}}{r^3} \tag{24}$$

A relationship between $\tau_{\theta\theta}$ and τ_{rr} can be obtained from eqs. (23) and (24):

$$\tau_{\theta\theta} = -\frac{1}{2}\tau_{rr} \tag{25}$$

where $\tau_{\theta\theta}$ is the stress tensor in the direction of angle ϕ in polar coordinates. Substituting eq. (25) into eq. (11) yields

$$2P_g - 2P_f - \frac{4\sigma}{R} - 2\xi\ln\frac{S}{R} + 3\int_R^S \frac{\tau_{rr}}{r}dr = 0 \tag{26}$$

On the basis of the previous analysis, the governing equations of the bubble growth are given by

$$\begin{cases} 2P_g - 2P_f - \frac{4\sigma}{R} - 2\xi\ln\frac{S}{R} + 3\int_R^S \frac{\tau_{rr}}{r}dr = 0 \\ \tau_{rr} + \lambda\left[\frac{\partial\tau_{rr}(r,t)}{\partial t} + \frac{R^2\dot{R}}{r^2}\frac{\partial\tau_{rr}(r,t)}{\partial r}\right] = -2\eta\frac{R^2\dot{R}}{r^3} \end{cases} \tag{27}$$

To facilitate the theoretical analysis, the following Lagrangian coordinate transformation[7,19] was used

$$h = \left[r^3 - R(t)^3\right] \tag{28}$$

where h is the Lagrangian coordinate radius. The parameter k_0 is defined as

$$k_0 = S^3 - R^3 = S_0^3 - R_0^3 \tag{29}$$

where k_0 is a constant because the melt shell volume is invariable because of its incompressible properties.

After Lagrangian transformation, eq. (23) can be rewritten as

$$\frac{\partial\tau_{rr}(h,t)}{\partial t} + \frac{\tau_{rr}(h,t)}{\lambda} = \frac{2\eta}{\lambda}\frac{R^2\dot{R}}{h+R^3} \tag{30}$$

Calculating eq. (30) leads to

$$\tau_{rr}(h,t) = \tau_{rr,0}e^{-\frac{t}{\lambda}} - \frac{2\eta}{\lambda}\int_0^t e^{\frac{\tau-t}{\lambda}}\frac{R^2\dot{R}}{h+R^3}d\tau \tag{31}$$

in which $\tau_{rr,0}$ (the initial normal stress) is $\tau_{rr}(h,0)$.

Substituting eq. (31) into eq. (26) results in

$$\begin{aligned} &2P_g - 2P_f - \frac{4\sigma}{R} - 2\xi\ln\frac{S}{R} + 3\int_R^S \frac{\tau_{rr}}{r}dr \\ &\quad = 2P_g - 2P_f - \frac{4\sigma}{R} - 2\xi\ln\frac{S}{R} + \int_0^{k_0}\frac{1}{h+R^3}\tau_{rr,0}e^{-\frac{t}{\lambda}}dh \\ &\qquad - \frac{2\eta}{\lambda}\int_0^{k_0}\frac{1}{h+R^3}dh\int_0^t e^{\frac{\tau-t}{\lambda}}\frac{R^2\dot{R}}{h+R^3}d\tau = 0 \end{aligned} \tag{32}$$

Equation (32) is discretized and simplified as followed

$$\begin{aligned} R_{n+1} &= R_n + \frac{R_n\lambda(k_0+R_n^3)}{\eta k_0} \\ &\times\left[P_{gn} - P_{fn} - \frac{2\sigma}{R_n} - \frac{1}{3}\xi\ln\frac{k_0+R_n^3}{R_n^3} + \frac{1}{2}\tau_{rr,0}e^{-\frac{t_n}{\lambda}}\ln\frac{k_0+R_n^3}{R_n^3}\right] \\ &\qquad - R_n e^{-\frac{\Delta t}{\lambda}}I_n \end{aligned} \tag{33}$$

where Δt is the time increment for each step, I_n is the value of equation (34) in step n after discretization, and n is the discretization number.

$$I_n = e^{-\frac{t_n}{\lambda}}\int_0^{t_n}\frac{e^{\frac{\tau}{\lambda}}\dot{R}(\tau)}{R(\tau)}d\tau = e^{-\frac{\Delta t}{\lambda}}I_{n-1} + \frac{R_n - R_{n-1}}{R_{n-1}} \tag{34}$$

Solution procedure

Dimensionless form of the governing equations

To facilitate the analysis, we defined the following dimensionless parameters and groups (denoted by an asterisk):

$$R^* = \frac{R}{R_0},\ t^* = \frac{t}{\lambda},\quad S^* = \frac{S}{R_0},\ k_0^* = \frac{k_0}{R_0^3},\ P_g^* = \frac{P_g}{P_a},$$
$$P_f^* = \frac{P_f}{P_a},\ \sigma^* = \frac{\sigma}{R_0 P_a},\ \xi^* = \frac{\xi}{P_a},\ \tau_{rr,0}^* = \frac{\tau_{rr,0}}{P_a},\ C_1 = \frac{\lambda P_a}{\eta}$$

where P_a is the ambient atmospheric pressure, R_0 is the initial bubble radius, and S_0 is the initial outer radius of the cell shell.

In terms of the dimensionless variables, eqs. (33) and (34) take the following forms

$$R_{n+1}^* = R_n^* + \frac{R_n^* C_1 (k_0^* + R_n^{*3})}{k_0^*} \times \left[P_{gn}^* - P_{fn}^* - 2\sigma_n^* * - \frac{1}{3}\xi^* \ln \frac{k_0^* + R_n^* 3}{R_n^{*3}} + \frac{1}{2}\tau_{rr,0}^* e^{-t_n^*} \ln k_0^* + R_n^{*3} n^{*3} \right] - R_n^* e^{-\Delta t^*} I_n \quad (35)$$

$$I_{n-1} = e^{-\Delta t^*} I_{n-2} + \frac{R_{n-1}^* - R_{n-2}^*}{R_{n-2}^*} \quad (36)$$

Parameter values

Melt strength. The melt strength of a PP resin is measured on a capillary rheometer.[20] The dependence of the melt strength on the temperature is given by[21]

$$\log(MS_N) = \frac{E}{R_g T} + \log C_S \quad (37)$$

where C_S is a constant, E is the activation energy of the melt strength (J/mol), and R_g is the molar gas constant.

The melt tension is defined as the melt strength per unit area and can be calculated with the following equation:

$$\xi = \frac{MS_N}{A} \quad (38)$$

where ξ is the melt tension and A is the area. The material constants for the CO_2/PP resin are listed in Table I for this study.[22–28]

P_f. With respect to ref. 18, P_f dropped from the initial ambient pressure (P_{f0}) to P_a within 3 s following the equation:

$$P_f = a + \frac{b}{(t+1)^3} \quad (39)$$

The initial and boundary conditions are

TABLE I
Basic Constants Required for the CO_2/PP System[22–28]

Initial bubble radius[22,25]	R_0	1 μm
Initial outer radius of the cell shell[24]	S_0	50 μm
Initial ambient pressure around the cell shell	P_{f0}	4.9725×10^6 N/m^2
Initial gas pressure inside the bubble[24]	P_{g0}	5×10^6 N/m^2
Surface tension[26]	σ	2.31×10^{-2} N/m
Initial normal stress[5,17]	$\tau_{rr,0}$	3.2×10^3 N/m^2
Initial gas concentration[28,35]	C_0	5%
Molar gas constant[24]	R_g	8.3143 J/mol K
Diffusion coefficient[24]	D	8×10^{-9} m^2/s
Henry's law constant[14,22–24]	K_h	1×10^{-8} m^2/N
Relaxation time[24]	λ	0.01 s
Viscosity	η	18,000 Pa s
Constant	C_S	4.02×10^{-15}
Activation energy	E	4.923×10^4 J/mol

P_{f0}, η, C_S, and E were calculated and measured in this study.

$$t = 0,\quad P_f = P_{f0}$$
$$t = 3,\quad P_f = P_a$$

P_{f0} was calculated with the equation:

$$P_{g0} - P_{f0} - \frac{2\sigma}{R_0} - \frac{1}{3}\xi^* 1n \frac{k_0 + R_0^3}{R_0^3} + \frac{1}{2}\tau_{rr,0} \ln \frac{k_0 + R_0^3}{R_0^3} = 0 \quad (40)$$

Initial gas pressure inside the bubble (P_{g0}). With respect to ref. 24, P_{g0} is expressed as

$$P_{g0} = \frac{C_0}{K_h} = \frac{5\%}{1 \times 10^{-8}} = 5 \times 10^6 = 5\ \text{MPa} \quad (41)$$

where C_0 is the initial gas concentration in the analyzed region.

Initial outer radius of the cell shell (S_0). The initial outer radius of the cell shell is given by[24]

$$S_0 = \left(\frac{3}{4\pi N_0}\right)^{\frac{1}{3}} (\text{cm}) \quad (42)$$

where N_0 is the cell density. When N_0 is in the range 10^8–10^9cells/cm^3, S_0 is 30 μm ~ 60 μm. In this study, S_0 was assumed to be 50 μm.

RESULTS AND DISCUSSION

Three parameters were taken into account in the bubble growing process on the basis of the previous controlling equations in this article, including the melt strength, viscoelasticity, and P_{g0}, as shown in Figures 2, 3, and 4. The three figures show that the bubble grew rapidly, accompanied by oscillation, during the early stage of bubble growth. Bubble oscillation is a common phenomenon in the bubble

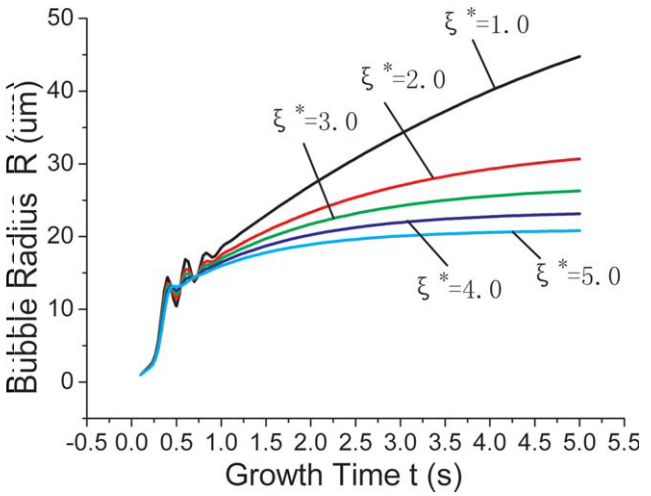

Figure 2 Bubble radius as a function of growth time for different dimensionless melt tensions ($C_1 = 0.05$, $P_{g0} = 5 \times 10^6$ N/m^2). [Color figure can be viewed in the online issue, which is available at www.interscience.wiley.com.]

growing process. Yang and Lawson,[29] Hoo and Han,[30] and Liu[31] reported that the bubble oscillates in the bubble growing process because the polymer melt has mass and elasticity. At the beginning of bubble growth, the bubble expands rapidly, and the polymer melt around the bubble flows outward in the radial direction, driven by the high P_g. P_g quickly drops because little gas diffuses into the bubble from the ambient melt within a very short time. P_g approaches the surrounding pressure bit by bit. Then, P_g keeps on dropping because of the continuous bubble growth because of inertia.[31,32] When P_g is lower than the pressure of the melt shell around the bubble, the melt flows inward, and the bubble shrinks. P_g increases because of gas diffusion and pressurization, which leads to bubble expansion for the second time. Then, the second cycle of bubble growth begins. The bubble oscillation persists permanently until the force becomes balanced or the energy is exhausted.

Figure 2 shows the effect of the dimensionless melt tension on the bubble growth. The melt tension is the melt strength per unit area, so Figure 2 also directly indicates the effect of the melt strength on bubble growth. The melt strength had little effect on the bubble growth rate during the early stage of bubble growth. However, the bubble oscillation amplitude was lower for the polymer with a higher melt strength. Furthermore, the oscillation attenuation accelerated as the melt strength increased. On the other hand, a higher melt strength led to a lower bubble growth rate, shorter growth time, and smaller ultimate bubble size in the latter stage of bubble growth. The melt strength is the resistance force to the melt tensile force and melt deformation. In the polymer foaming process, a higher melt strength implies a higher resistance to bubble growth and a higher damp force for the bubble oscillation. Therefore, a high melt strength is very useful for stabilizing bubble oscillation and decreasing the bubble size, which is very important for microcellular foaming. On the basis of the previous analysis, we concluded that the melt strength is a very important parameter for bubble growth in the foaming process, especially for semicrystalline polymers, such as PP and polyethylene (PE). PP resin has a very poor foamability, mainly because of its low melt strength, because of the linear molecular structure and crystallizable properties. Several methods

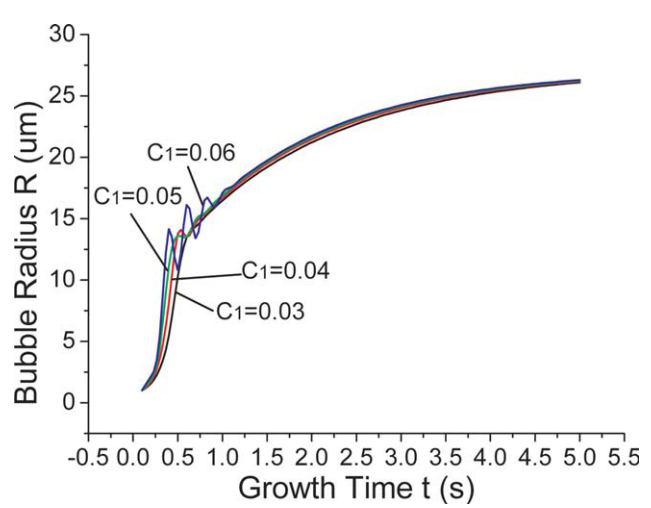

Figure 3 Bubble radius as a function of growth time for different values of C_1^* ($P_{g0} = 5 \times 10^6$ N/m^2, $\xi^* = 3.0$). [Color figure can be viewed in the online issue, which is available at www.interscience.wiley.com.]

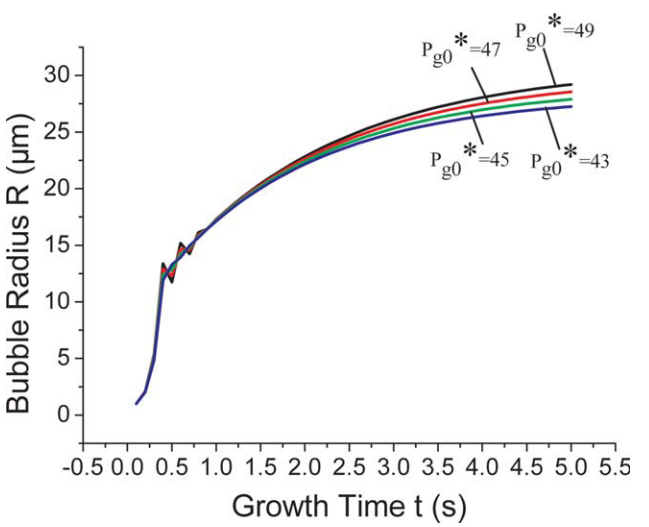

Figure 4 Bubble radius as a function of growth time for different values of P_{g0}^* (where $P_{g0}^* = P_{g0}/P_a$, $C_1 = 0.05$, $\xi^* = 3.0$). [Color figure can be viewed in the online issue, which is available at www.interscience.wiley.com.]

have been used to enhance the melt strength and improve the foamability of PP.[33–35]

Figure 3 shows the bubble growth as a function of growth time for different dimensionless parameters (C_1^*'s). C_1 is the ratio of elasticity to viscosity of the polymer ($C_1 = \lambda P_a/\eta$), which reflects the polymer viscoelasticity, where λ is the relaxation time relating to the polymer elasticity. A longer λ implies a higher elasticity. A decreasing λ or increasing melt η leads to a decrease of C_1. The effect of C_1 on bubble growth is obvious in Figure 3. During the early stage of bubble growth, the bubble oscillation amplitude and bubble growth rate decrease, and the oscillation attenuation accelerates as C_1 decreases, which implies that the melt viscoelasticity is one of the resistances for the bubble growth. However, in the latter stage of bubble growth, C_1 has little effect on the growth rate and ultimate bubble size. A similar ultimate bubble radius was obtained with various C_1 values, as shown in Figure 3.

Figure 4 shows the effect of the P_{g0}^* on the bubble radius. The bubble growth rate varies little, but the bubble oscillation increases as P_{g0} increases in the early stage of bubble growth. In the latter stage, the bubble growth rate accelerates with increasing P_{g0}, which leads to an increase in the ultimate bubble radius. P_g is the main driving force for bubble growth. A higher P_{g0} implies a larger driving force, which leads to easier bubble growth, a higher growth rate, and bubble oscillation, as shown in Figure 4.

CONCLUSIONS

The effects of the melt strength, viscoelasticity, and gas pressure on bubble growth were studied and simulated in theory on the basis of mechanical analysis of the bubble growth with a cell model. We made the following conclusions:

1. The theoretical analysis indicated that the bubble grows rapidly accompanied by oscillation in the early stage of bubble growth.
2. The effect of the melt strength on the bubble growth was thoroughly and theoretically investigated in this study. The oscillation amplitude decreases and the oscillation attenuation accelerates with increasing melt strength in the early stage of bubble growth. During the latter stage, the bubble growth rate and growth time greatly decrease as the melt strength increases, which leads to a diminishment in ultimate bubble size. Therefore, the melt strength plays a very important role in stabilizing bubble growth and decreasing the ultimate bubble size.
3. The polymer viscoelasticity has less influence on bubble growth. As C_1^* decreases, the bubble oscillation amplitude and bubble growth rate decrease, and the oscillation attenuation accelerates during the early stage of bubble growth. However, in the latter stage, the growth rate and ultimate bubble size vary little as C_1 decreases.
4. P_g is the driving force for the bubble growth. An increasing P_{g0} leads to an enhancement in the bubble oscillation and bubble growth rate, so the ultimate bubble size increases.

References

1. Goutille, Y.; Guillet, J. Soc Rheol 2002, 46, 1307.
2. Lee, C. H.; Lee, K.-J.; Jeong, H. G.; Kim, S. W. Adv Polym Technol 2000, 19, 97.
3. Yang, W. J.; Yeh, H. C. AIChE J 1966, 12, 927.
4. Shima, A.; Tsujino, T. Chem Eng Sci 1976, 31, 861.
5. Han, C. D.; Yoo, H. J. Polym Eng Sci 1981, 21, 518.
6. Arefmanesh, A.; Advani, S. G.; Michaelides, E. E. Polym Eng Sci 1990, 30, 1330.
7. Arefmanesh, A.; Advani, S. G. Rheol Acta 1991, 30, 274.
8. Amon, M.; Denson, C. D. Polym Eng Sci 1984, 24, 1026.
9. Zana, E.; Leal, L. G. Ind Eng Chem Fundam 1975, 14, 175.
10. Joshi, K.; Lee, J. G.; Shafi, M. A.; Flumerfelt, R. W. J Appl Polym Sci 1998, 67, 1353.
11. Feng, J. J.; Bertelo, C. A. Soc Rheol 2003, 48, 439.
12. Yang, K.; Cao, X.; Cao, Z. The Interface and Film and Their Application; Science Publishing Firm: Beijing, 1989.
13. Guo, L. Hydrodynamics of the Two and Multi-Phases; Xi'An JiaoTong University Publishing Firm: Xi An, China, 2002.
14. Shafi, M. A.; Flumerfelt, R. W. Chem Eng Sci 1997, 52, 627.
15. Shafi, M. A.; Lee, J. G.; Flumerfelt, R. W. Polym Eng Sci 1996, 36, 1950.
16. Tuladhar, T. R.; Mackley, M. R. Chem Eng Sci 2004, 59, 5997.
17. Wu, H. M.S. Thesis, South China University of Technology, 2005.
18. Tian, S. Ph.D. Dissertation, South China University of Technology, 1999.
19. Goel, S. K.; Bechman, E. J. AIChE J 1995, 41, 357.
20. Muke, S. J Non-Newtonian Fluid Mech 2001, 101, 77.
21. Lau, H. C.; Bhattacharya, S. N.; Field, G. J. Polym Eng Sci 1998, 38, 1915.
22. Tuladhar, T. R.; Mackley, M. R. Chem Eng Sci 2004, 59, 5997.
23. Shafi, M. A.; Joshi, K.; Flumerfelt, R. W. Chem Eng Sci 1997, 52, 635.
24. Otsuki, Y.; Kanai, T. Polym Eng Sci 2005, 1277.
25. Osorio, A.; Turng, L.-S. Polym Eng Sci 2004, 44, 2274.
26. Kwok, D. Y.; Cheung, L. K.; Park, C. B.; Neumann, A. W. Polym Eng Sci 1998, 38, 757.
27. Han, C. D.; Yoo, H. J. Polym Eng Sci 1981, 21, 518.
28. Doroudiani, S.; Park, C. B.; Kortschot, M. T. Polym Eng Sci 1998, 38, 1205.
29. Yang, W. J.; Lawson, M. L. J Appl Phys 1974, 45, 754.
30. Hoo, H. J.; Han, C. D. AIChE J 1982, 28.
31. Liu, X. P. Ph.D. Dissertation, South China University of Technology, 2000.
32. Jimenez-Fernandez, J.; Crespo, A. Ultrasonics 2005, 43, 643.
33. Nakajima, Y.; Kimura, T.; Nagaoka, Y.; B1, E. P. Eur. Pat. 0287011B1 (1988).
34. Naguib, H. E.; Park, C. B.; Reichelt, N.; Panzer, U. Polym Eng Sci 2002, 42, 1481.
35. Park, C. B.; Cheugn, L. K. Polym Eng Sci 1997, 37, 1.